



Author

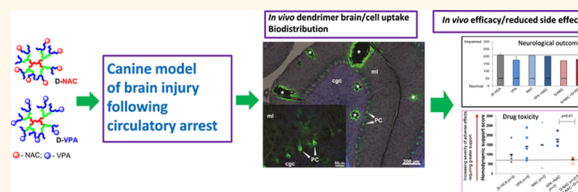
# Dendrimer Brain Uptake and Targeted Therapy for Brain Injury in a Large Animal Model of Hypothermic Circulatory Arrest

Manoj K. Mishra,<sup>†,▽</sup> Claude A. Beaty,<sup>‡,▽</sup> Wojciech G. Lesniak,<sup>†</sup> Siva P. Kambhampati,<sup>†</sup> Fan Zhang,<sup>†</sup> Mary A. Wilson,<sup>§,||</sup> Mary E. Blue,<sup>§,||</sup> Juan C. Troncoso,<sup>§,¶</sup> Sujatha Kannan,<sup>||,#</sup> Michael V. Johnston,<sup>§,||,△</sup> William A. Baumgartner,<sup>‡,▼,\*</sup> and Rangaramanujam M. Kannan<sup>†,▼,\*</sup>

<sup>†</sup>Center for Nanomedicine/Wilmer Eye Institute, Department of Ophthalmology, Johns Hopkins School of Medicine, Baltimore, Maryland 21287, United States,

<sup>‡</sup>Division of Cardiac Surgery, <sup>§</sup>Department of Neurology, and <sup>||</sup>Department of Neuroscience, The Johns Hopkins Medical Institutions, Baltimore, Maryland 21287, United States, <sup>¶</sup>Hugo W. Moser Research Institute at Kennedy Krieger, Inc., Baltimore, Maryland 21205, United States, and <sup>△</sup>Division of Neuropathology, <sup>#</sup>Department of Anesthesiology and Critical Care Medicine, and <sup>△</sup>Department of Pediatrics, The Johns Hopkins Medical Institutions, Baltimore, Maryland 21287, United States. <sup>▽</sup>Equal first authors. <sup>\*</sup>Equal senior authors.

**ABSTRACT** Treatment of brain injury following circulatory arrest is a challenging health issue with no viable therapeutic options. Based on studies in a clinically relevant large animal (canine) model of hypothermic circulatory arrest (HCA)-induced brain injury, neuroinflammation and excitotoxicity have been identified as key players in mediating the brain injury after HCA. Therapy with large doses of valproic acid (VPA) showed some neuroprotection but was associated with adverse side effects. For the first time in a large animal model, we explored whether systemically administered polyamidoamine (PAMAM) dendrimers could be effective in reaching target cells in the brain and deliver therapeutics. We showed that, upon systemic administration, hydroxyl-terminated PAMAM dendrimers are taken up in the brain of injured animals and selectively localize in the injured neurons and microglia in the brain. The biodistribution in other major organs was similar to that seen in small animal models. We studied systemic dendrimer–drug combination therapy with two clinically approved drugs, *N*-acetyl cysteine (NAC) (attenuating neuroinflammation) and valproic acid (attenuating excitotoxicity), building on positive outcomes in a rabbit model of perinatal brain injury. We prepared and characterized dendrimer-NAC (D-NAC) and dendrimer-VPA (D-VPA) conjugates in multigram quantities. A glutathione-sensitive linker to enable fast intracellular release. In preliminary efficacy studies, combination therapy with D-NAC and D-VPA showed promise in this large animal model, producing 24 h neurological deficit score improvements comparable to high dose combination therapy with VPA and NAC, or free VPA, but at one-tenth the dose, while significantly reducing the adverse side effects. Since adverse side effects of drugs are exaggerated in HCA, the reduced side effects with dendrimer conjugates and suggestions of neuroprotection offer promise for these nanoscale drug delivery systems.



**KEYWORDS:** PAMAM dendrimers · cardiac arrest · canine model · brain injury · biodistribution · combination therapies · neuroinflammation · cytotoxicity · valproic acid · *N*-acetylcysteine

**N**eurological injury after cardiac surgery, particularly after hypothermic circulatory arrest (HCA), remains a major and persistent problem.<sup>1</sup> The technique of hypothermic circulatory arrest (HCA) is an established neuroprotective strategy allowing complex repairs of the thoracic aorta and congenital cardiac malformations, but many patients exhibit significant neurological sequelae, including intellectual and neuropsychomotor impairment, seizures, choreoathetosis, delayed development, and stroke. Although only

1–3% of patients undergoing routine cardiac surgery have strokes, many experience neurocognitive dysfunction,<sup>2–4</sup> and neurological complications are more common after repair of complex aortic lesions and congenital malformations.<sup>5,6</sup> HCA has been the cornerstone for neuroprotection during repair of aortic lesions and congenital heart defects since 1950.<sup>7–9</sup> Although 45–60 min of HCA is generally considered safe, neurologic complications include stroke, seizures, neurocognitive dysfunction, and delayed neuropsychomotor development.<sup>6,10–12</sup> Despite over

\* Address correspondence to  
krangar1@jhmi.edu,  
wbaumgar@jhmi.edu.

Received for review September 17, 2013  
and accepted February 5, 2014.

Published online February 05, 2014  
10.1021/nn404872e

© 2014 American Chemical Society

60 years of research, no therapeutic intervention has proven to consistently protect against HCA-induced neurological dysfunction. This is partly due to the fact that animal models of HCA-associated brain injury that are representative of the injury in humans are challenging and can be created only in large animals, making them very expensive for fundamental studies.

Baumgartner and co-workers developed the clinically relevant canine model of HCA-induced brain injury used in the current study to elucidate the mechanisms and neurological consequences of brain injury. They have shown that excitotoxicity and neuroinflammation are critical mediators of post-HCA neurological injury, and that the drug valproic acid (VPA) partially mitigates excitotoxic injury.<sup>13,14</sup> However, the doses required to achieve neuroprotection induce severe adverse effects such as metabolic acidosis and hypotension in humans, limiting its clinical use [unpublished results]. *N*-Acetylcysteine (NAC) is effective in reducing neuroinflammation but exhibits poor blood-brain barrier (BBB) penetration and inadequate brain localization, requiring large doses to achieve neuroprotection.<sup>15–18</sup> Moreover, hypothermia and circulatory arrest increase drug toxicity and worsen adverse effects of drugs, even at doses that are normally well-tolerated, due to alterations in drug clearance and in drug response.<sup>19–21</sup> Therefore, we adopted a strategy to attenuate both excitotoxicity and neuroinflammation, using combination, targeted therapies to maximize therapeutic effects while minimizing side effects. This study explores the potential of polyamidoamine (PAMAM) dendrimers, utilizing their ability to selectively localize in cells associated with neuroinflammation.<sup>22–25</sup> These are the first large-animal-based therapeutic studies with PAMAM dendrimers.

**Excitotoxicity in HCA.** Glutamate excitotoxicity is an important mediator of cell death after HCA, as demonstrated by both post-mortem histology and protective effects of glutamate receptor inhibition.<sup>26,27</sup> Hypoxic-ischemia during HCA triggers excessive release of the major excitatory neurotransmitter glutamate and overactivation of glutamate receptors, particularly *N*-methyl-D-aspartate (NMDA) receptor-gated ion channels. This precipitates a cascade of intracellular events leading to cell death, particularly in the hippocampus.<sup>26,27</sup> These events include high intracellular  $\text{Ca}^{2+}$  levels, which triggers apoptotic cell death through a variety of downstream effectors.<sup>28–30</sup> Ischemia also induces persistent changes in mitochondrial metabolism resulting in increased cerebral lactate levels.<sup>31,32</sup>

**Inflammation in HCA.** Neuroinflammation is also an important mediator of neurological injury after HCA. Both cardiopulmonary bypass (CPB) and HCA are associated with significant, prolonged systemic inflammatory responses after cardiac surgery.<sup>33</sup> Elevated markers of inflammation, including C-reactive protein and interleukin-6 (IL-6), correlate with prolonged neurocognitive

dysfunction.<sup>34,35</sup> Additionally, inflammatory events lead to the expression of high systemic levels of tumor necrosis factor- $\alpha$  (TNF- $\alpha$ ) that disrupts the blood-brain barrier and allows many compounds that are normally limited to the periphery to enter the brain.<sup>36,37</sup> Thus systemic inflammation contributes to neuroinflammation, which can then lead to neurocognitive dysfunction.<sup>38,39</sup>

Microglia, the resident macrophages of the central nervous system, detect brain injury and initiate neuroinflammation. Microglia are rapidly activated in response to a wide range of injuries, including ischemic, infectious, traumatic, autoimmune, and degenerative processes; ischemia-reperfusion injury induces microglial activation in the hippocampus as early as 20 min after reperfusion.<sup>40–42</sup> Activated microglia release multiple cytotoxic compounds, including reactive oxygen species (ROS), inflammatory cytokines and glutamate.<sup>23,43,44</sup> Thus, HCA-induced ischemia triggers both excitotoxicity and neuroinflammation that function synergistically to produce neuronal cell death and further microglial activation. Because microglial activation can cause both neuronal excitotoxicity and neuroinflammation, attenuation of microglial activity represents a promising avenue to ameliorate post-HCA injury. This study compares single and combined free drug treatment and targeted nanotherapies aimed at both of these important mechanisms of injury after HCA.

Dendrimers are promising candidates for imaging and targeted drug/gene delivery in cancer and in systemic and CNS inflammation.<sup>23–25,45–48</sup> Interestingly, we have also shown that hydroxyl-functionalized generation-4 PAMAM dendrimers (4 nm, 14 kDa, nearly neutral, containing no targeting moieties) selectively localize in activated microglia in the injured brain and retina.<sup>23–25</sup> The generation-4, hydroxyl-terminated, polyamidoamine dendrimers used in this study are noncytotoxic in small animal models, even up to 500 mg/kg doses.<sup>23</sup> The noncytotoxic nature of this dendrimer may be attributable to its neutral surface, which does not cause protein opsonization or blood hemolysis, and the fact that it is cleared intact through the urine.<sup>23,47–49</sup> Previous studies showed minimal brain uptake of PAMAM dendrimers in healthy and tumor-xenograft-bearing animals.<sup>22,46–49</sup> However, neuroinflammation impairs the BBB,<sup>23,50,51</sup> and we have shown that PAMAM dendrimers are taken up by the brain in the presence of inflammation.<sup>23</sup> In a rabbit model of cerebral palsy (CP), we showed that these dendrimers diffuse rapidly in the brain tissue and localize selectively in activated microglia. Importantly, dendrimer-NAC (D-NAC) conjugates produced dramatic motor function improvement and attenuated neurological injury.<sup>23</sup> We have also shown successful targeting of microglia for neuroprotection in retinal degeneration.<sup>25</sup> Since these generation-4 PAMAM dendrimers are cleared from the off-target organs and the whole body relatively quickly, side effects may be reduced, compared to free drugs.

Building on the positive efficacy results in a small animal brain injury model,<sup>23</sup> we explored therapy using dendrimers in this clinically relevant large animal brain injury model. The objectives were to see if (a) systemically administered dendrimers would be transported to the injured brain with a similar cellular localization as seen in local intracisternal administration; (b) combination therapy using a lower dose of the conjugated drug leads to an equivalent improvement in neurological scores as seen with the use of larger doses of free drugs; and (c) combination therapy with dendrimer–drug conjugates would reduce the hemodynamic side effects associated with the large doses required to show efficacy for the free drugs. The free drug doses selected for these studies were based on previously published results from our group and others demonstrating neuroprotection,<sup>13</sup> and this VPA dose produced serum levels that are therapeutic in humans for seizure control. These are the first dendrimer studies in a large animal brain injury model. Although these efficacy results are preliminary, this study highlights the potential for use of dendrimer–drug therapies in this translationally relevant large animal model, while also validating our ability to make dendrimer–drug conjugates on a large scale using two clinically approved drugs.

## RESULTS AND DISCUSSION

**Systemically Administered PAMAM Dendrimers (D-FITC) Are Taken up in the Injured Brain and Localize in Activated Microglia and Injured Neurons after HCA.** We hypothesized that the brain injury following HCA impairs the blood-brain barrier in injured regions of the brain. To detect breakdown of the BBB, immunohistochemistry was used to detect immunoglobulin G (IgG), a large serum protein that does not cross an intact BBB but can cross a disrupted BBB. IgG staining was assessed in sections passing through parietal and cingulate cortex and the hippocampus in normal controls (Figure 1A) and at 2, 8, and 24 h after HCA (Figure 1B,C). Although there was marked variation from animal to animal, IgG extravasation was observed in restricted areas of cerebral cortex (Figure 1B) and hippocampus (Figure 1C), 8–24 h after HCA, typically in areas where injury is observed in H&E samples. These findings are consistent with cDNA microarray analysis of mRNA expression showing increased matrix metallopeptidase 2 (MMP2), MMP9, and MMP3, which digest barrier proteins such as occludin and claudin 5, leading to BBB breakdown (data not shown). These findings suggest that systemically administered therapy with drugs and dendrimer–drug conjugates is likely to enter injured brain tissue, regardless of their cerebral bioavailability with an intact BBB.

We have previously described the synthesis, purification, and characterization of D-FITC and D-Cy5 conjugates.<sup>23,25,52–54</sup> We characterized the kinetics and biodistribution of fluorescently labeled dendrimers

in the HCA model after IV administration. In these experiments, D-FITC was injected intravenously after 2 h of hypothermic circulatory arrest. Tissues were harvested 48 h after dendrimer administration to study uptake and retention. In brain tissue, IV-injected D-FITC was selectively taken up in the injured hippocampal dentate granule cell layer (Figure 1D), in cerebellar Purkinje and granule neurons, and in microglia (Figure 1F). These neurons receive the major glutamatergic input to hippocampus from entorhinal cortex and are highly vulnerable to injury after HCA.<sup>26,27</sup> Greater uptake in the more severely injured HCA animal, compared to the “noninjured” control cardiopulmonary bypass (CPB) animal (Figure 1E), was confirmed by fluorescence microscopy (Figure 1D,F) and suggests that dendrimers cross the injured BBB and localize in injured cells after IV administration. Interestingly, dendrimers were localized in the superficial part of the dentate granule cell layer containing injured neurons and activated microglia (Figure 1D) but not in the deeper part of this layer, where most neurons in this subject were uninjured. A qualitative assessment of relative fluorescence intensity in sections of different brain regions revealed cerebellum > hippocampus > cerebral cortex, which is in agreement with the quantitative assays reported below and closely corresponds to the regional and cellular pattern of injury that is characteristic of this model.

The tissue biodistribution following administration into the cisterna magna of dendrimer-Cy5 was compared to that following intravenous administration of dendrimer-FITC in the same animal. D-Cy5 (ICM) and D-FITC (IV) were comparably distributed in the injured dentate granule cell layer (Supporting Information Figure S1) in cells with fragmented nuclei characteristic of apoptotic neurons. This suggests that selective neuronal uptake can be achieved through either route, and that the transport through the impaired BBB is not limiting in terms of qualitative brain biodistribution.

**Quantitative Biodistribution and Excretion of Brain-Administered Dendrimer-Cy5 and Systemically Administered Dendrimer-FITC.** We developed a sensitive method for tissue quantification of fluorescently labeled PAMAM dendrimers, with a 10 ng detection limit, using a combination of total fluorescence and high-performance liquid chromatography (HPLC) of tissue-extracted with fluorescence and photodiode array (PDA) detectors. The presence of conjugates in the CNS was confirmed using a combination of three independent measurements including fluorescence spectroscopy, HPLC, and size-exclusion chromatography (SEC). Figure S2 shows the emission spectra recorded for extracts obtained from kidneys of control dog (with no D-Cy5) and that from dogs treated with IV infusion of D-Cy5. A clear increase in the fluorescence intensity compared to control (tissue autofluorescence) was seen, which was quantified using calibration curve included in Figure S2. The same approach was used for

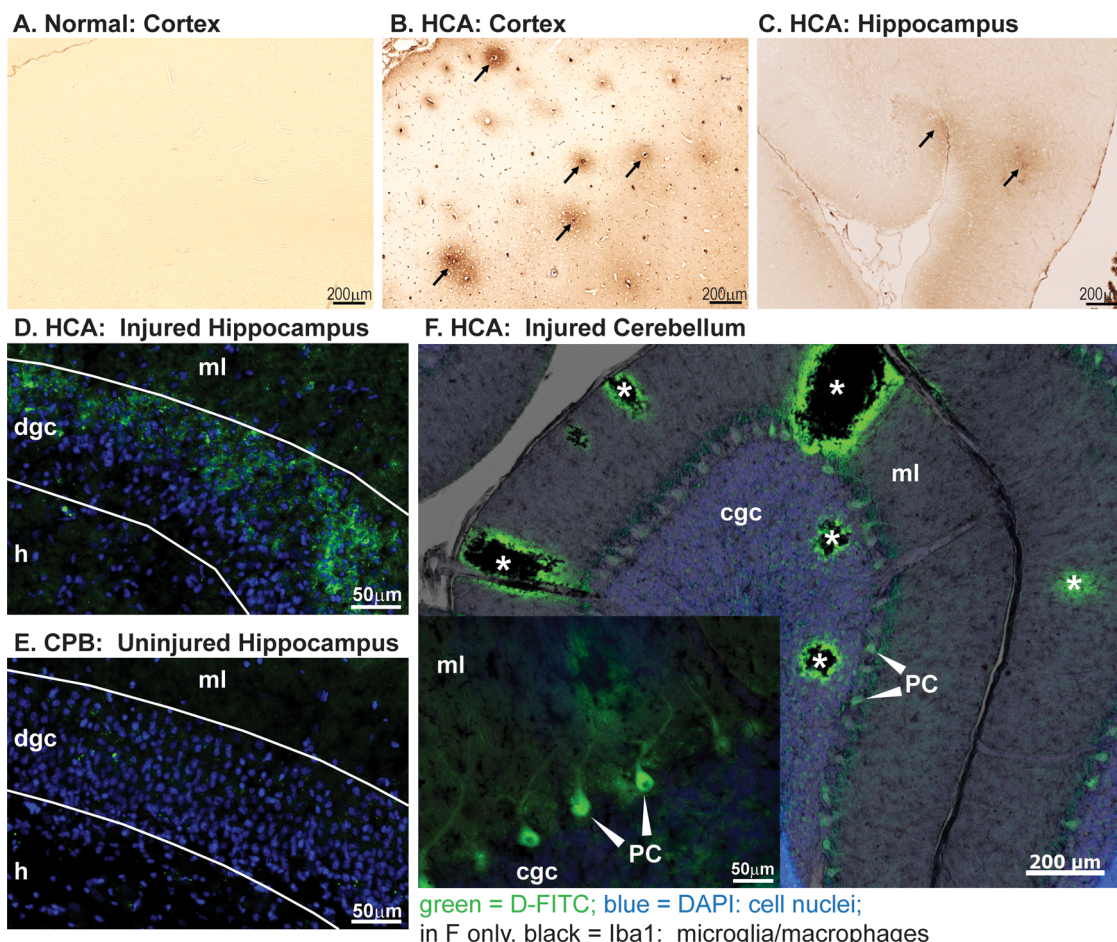


**Figure 1.** (A–C) Blood-brain barrier breakdown demonstrated by extravasation of IgG. To detect breakdown of the BBB, immunohistochemistry was used to detect IgG, a large serum protein that does not cross an intact BBB. (A) In a normal dog with intact BBB, IgG is not detected in cerebral cortex. (B) IgG extravasation can be seen surrounding many vessels (arrows) in the cerebral cortex of a dog euthanized 8 h after undergoing HCA. (C) More diffuse areas of IgG extravasation are apparent in the hippocampus of another dog euthanized 8 h after HCA. Although there was marked variation from animal to animal, IgG extravasation was observed in restricted areas of cerebral cortex and hippocampus, 8–24 h after HCA, typically in areas where injury is observed in H&E samples. The most striking examples are shown. (D–F) Systemically administered D-FITC localizes in injured brain cells. D-FITC was administered IV after 2 h HCA or CPB; fluorescent labeling was examined 48 h later. (D) D-FITC labeling in the outer part of the hippocampal dentate granule cell layer (dgc) after HCA closely corresponds to the distribution of apoptotic nuclei detected with DAPI. (E) Very little labeling is observed in hippocampus after CPB, which causes little to no injury. (F) In cerebellum after HCA, D-FITC is prominent in many Purkinje cells (PC), which receive dense glutamatergic input and are often injured, and surrounding small hemorrhages (\*). Fainter FITC labeling is present in the cerebellar granule cell layer (cgc), where apoptotic neurons are often observed after HCA (ml, molecular layer; h, hilus).

determination of both D-Cy5 and D-FITC conjugates in all analyzed specimens. In the case of IV- and ICM (brain)-administered D-Cy5, its presence in analyzed specimens was additionally validated by SEC (Figure S3) and HPLC (Figure S4), which are sensitive to the difference between free Cy5 (HPLC) and D-Cy5 (HPLC and SEC). Figure S4 illustrates a representative HPLC chromatogram obtained from D-Cy5, free dye, serum, kidney extracts, and urine. Results indicated that D-Cy5 and free dye exhibited different retention times and could be simultaneously analyzed by HPLC with UV-vis absorbance at 650 nm and fluorescence using excitation at 645 nm with emission at 665 nm. Under peaks related to D-Cy5 (broad peak between 10 and 15 min) and Cy5 (peaks at 16 and 18 min), the same UV-vis profile characteristic for the Cy5

dye was recorded, which confirmed its covalent attachment to the dendrimer. UV-vis spectra obtained within peaks were very useful in their assignment in chromatograms acquired for biological samples as illustrated for serum (Figures S3B and S4B), kidney extracts (Figures S3C and S4C), and urine (Figures S3D and S4D). In all analyzed specimens, only traces of free Cy5 were detected ( $\sim 3\%$ ), indicating low amounts of dye dissociation from the dendrimer during this time. In addition, conjugates and specimens were analyzed by a size-exclusion chromatography (Figure S3) with both PDA and fluorescence detectors. In accordance with HPLC, SEC also identified the presence of D-Cy5 in the blood serum, kidneys, and urine, providing peaks associated with the conjugate that had its spectroscopic and fluorescence signature.

**TABLE 1. Biodistribution of D-Cy5 (48 h Post-ICM Injection) and D-FITC (48 h Post-IV Infusion) in Brain, Different Organs, and Fluids of HCA Canine Model ( $n = 3$ )<sup>a</sup>**

brain region	ICM D-Cy5 (48 h PA)	IV D-Cy5 (6 h PA)	IV D-FITC (48 h PA)
cortex	6.3 ± 3.7	0.01	
cerebellum	5.8 ± 3.3	0.06	
hippocampus	6.5 ± 3.7	0.03	
organs			
Kidney	0.54 ± 0.43	99.43	61.2 ± 13.3
liver	0.07 ± 0.03	3.73	1.12 ± 0.4
heart	0.03 ± 0.01	0.28	1.25 ± 0.6
lung	0.11 ± 0.05	0.98	2.2 ± 1.1
pancreas	0.11 ± 0.06	1.75	0.9 ± 0.43
fluids			
CSF	7.2 ± 3.1	0.08	0.02 ± 0.01
serum	0.07 ± 0.03	3.5	7.0 ± 0.4
urine	0.37 ± 0.24	37.41	21.5 ± 2.2

<sup>a</sup> One dog was treated with D-Cy5 IV-infused for 1 h and sacrificed 6 h post-administration. Note: PA, post-administration. Both conjugates (D-Cy5, 0.015 g; and D-FITC, 0.140 g) were administered to the same dog. Accumulation of D-FITC in brain regions could not be quantified due to its low concentration and the autofluorescence in the FITC channel originating from the tissue, masking the presence of the conjugate in the sample. Therefore, IV D-Cy5 measurements were used for brain uptake since minimal tissue autofluorescence was observed in the Cy5 channel. Results are expressed in [ $\mu\text{g/g}$ ] for solid tissue and [ $\mu\text{g/mL}$ ] for fluids.

Importantly, analysis with the use of fluorescence was much quicker and 100-fold more sensitive compared to HPLC and SEC. Fluorescence spectroscopy was sensitive enough to detect D-Cy5 in brain samples at concentrations of 1 ng per gram of tissue. The same approach was used for determination of ICM-injected D-Cy5 and IV-infused D-FITC in three other dogs. Accumulation of the conjugates in the injured brain (cortex, hippocampus, cerebellum) and major peripheral organs is presented in Table 1. Results indicated the highest uptake of the conjugates by kidneys and their marginal accumulation in other major organs, which was in good agreement with clearance data (Figure 2), demonstrating the highest concentration of IV-administered dendrimers in the blood immediately after infusion. Collectively, biodistribution and clearance results obtained for IV-injected D-Cy5 (over 6 h) and D-FITC (over 48 h) indicated that dendrimers were efficiently and rapidly cleared from the bloodstream via the kidneys, with relatively low retention in other major organs. The highest concentration in blood and urine was seen immediately after infusion. Interestingly, their maximum level in the cerebrospinal fluid was observed 4–8 h post-infusion when there is evidence for disruption of the BBB (Figure 1); levels then significantly decreased in the next 18 h. On the other hand, ICM-injected D-Cy5 exhibited high local concentrations for 6 h after injection, which slowly decreased over time. Its concentration in the blood slowly increased up to 1.5 h post-injection and remained constant at all further time points measured,

suggesting gradual clearance of the dendrimer from the CSF. It was in good agreement with the level of D-Cy5 in urine, which increased within 1.5 h of ICM injection and remained stable for up to 48 h. As expected, the highest accumulation of ICM-injected D-Cy5 (6  $\mu\text{g/g}$  of tissue) was found in the analyzed brain regions, followed by kidneys. Brain uptake of intravenously injected D-Cy5 was 100 times lower, but clearly measurable (Table 1). IV-administered D-FITC was not measurable in the brain of these large animals, due to tissue autofluorescence in the brain at FITC wavelengths (Table 1). However, IV D-FITC was measurable in CSF by 30–60 min (0.2  $\mu\text{g/mL}$ ), peaked at 6–8 h (0.5  $\mu\text{g/mL}$ ), and mostly cleared by 48 h (0.06  $\mu\text{g/mL}$ ). Dendrimer biodistribution in all major organs (Table 1), serum ( $\sim$ 100  $\mu\text{g/mL}$  at 8 h and cleared in 24 h), and urine was also analyzed. Over the 24 h after administration, the CSF/serum ratio for the dendrimer was approximately 1%. Dendrimer retention by other major organs at 48 h was relatively low, with its highest tissue accumulation in kidneys (~8%), suggesting that off-target cytotoxic effects were unlikely.<sup>6</sup> This is a critical factor in this model since free drugs showed adverse systemic side effects that prevented translation. Dendrimer biodistribution in nonbrain tissue and clearance in the HCA dog model were in good agreement with published data for other small animal models measured with radiolabeled dendrimers.<sup>22,46–49</sup> Fluorescence quantification had high sensitivity, allowed assessment of uptake in different brain regions and other tissues, and was more practical than radiolabeling in this large animal model. It also allowed for cellular imaging of dendrimers. The brain uptake and retention levels of the dendrimers, even though small, were qualitatively higher than the levels of free NAC in the brain in small animal models.

**Preparation of Dendrimer-NAC (D-NAC) and Dendrimer-VPA (D-VPA) Conjugates on a Multigram Scale.** In this large animal model, the severity of the injury and the associated animal handling considerations mandated that the dogs survive only to 72 h after the HCA injury. The conjugates had to reach the brain, target microglial cells and injured neurons, release the drug(s) rapidly, and effect a therapeutic response over 24–72 h. Therefore, a rapid drug release strategy was not only required but also clinically important since most of the injury occurs around the time of and immediately after the procedure. Moreover, in this type of brain injury, the timing of the injury is well-known and hence the therapies can be timed accordingly. Therefore, we chose a disulfide-based linker, which will trigger a rapid intracellular release in the presence of high intracellular glutathione (GSH) levels. We have previously validated this approach for D-NAC conjugates,<sup>55,56</sup> and the same strategy was used in these studies.

**Preparation and Characterization of the Bifunctional Dendrimer (2).** We used generation-4 PAMAM dendrimer

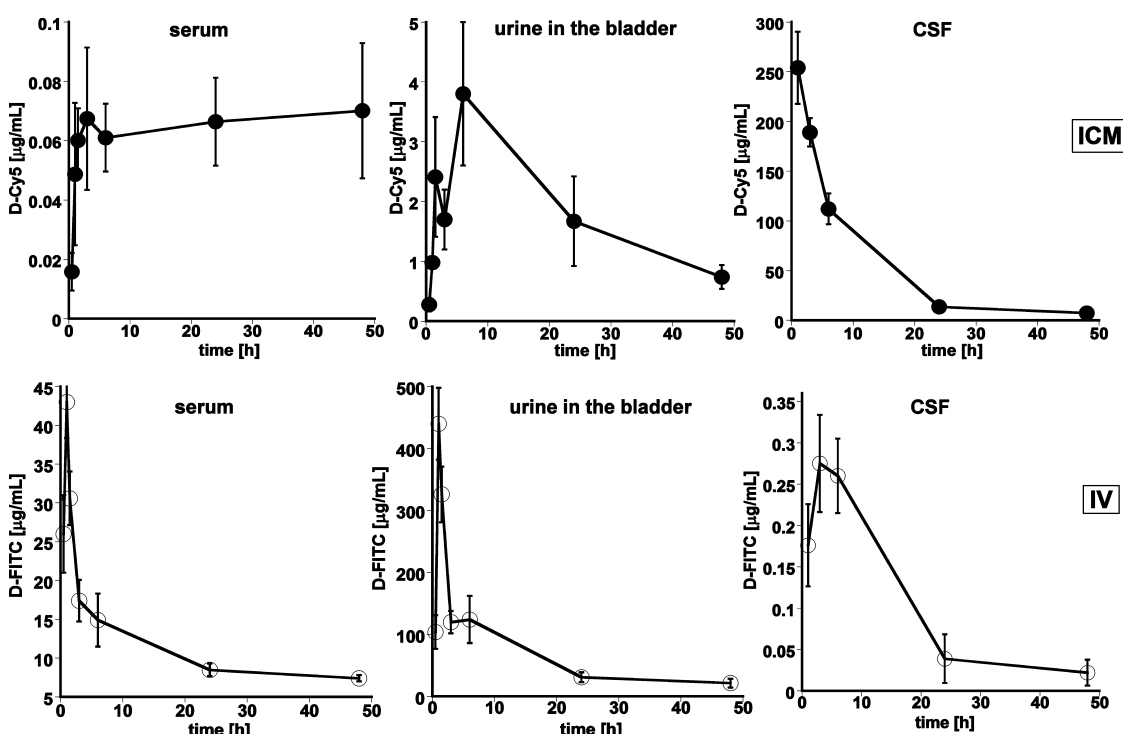


**Figure 2.** Concentrations of D-Cy5 (ICM administration, top), and D-FITC (IV infusion, bottom) in serum, urine from bladder, and cerebrospinal fluid (CSF). The conjugates were administered simultaneously after 2 h HCA, and the dogs were euthanized 48 h post-administration ( $n = 3$ ).

(G4-OH) due to its significantly improved toxicity profile compared to the amine counterpart. In an attempt to prepare D-VPA and D-NAC conjugates, the G4-OH was functionalized with amines to further react with SPDP linker and drug. Previously, we reported the synthesis of bifunctional dendrimers in 100 mg quantities.<sup>23,55</sup> The drug doses and the use in a large animal (30 kg) required us to prepare  $\sim$ 4 g of conjugates for each animal. We developed a large-scale (4–5 g) synthetic procedure for a large canine model and validated its yield, purity, and the number of linkers reacted to the surface of the dendrimer.

A bifunctional dendrimer (**2**) was prepared with a goal to react 20–25 NH<sub>2</sub> groups on the surface of the dendrimer using Fmoc protection/deprotection chemistry shown in Figure 3A.<sup>52</sup> Fmoc-GABA-OH was reacted with the dendrimer using PyBOP as a coupling reagent to produce Fmoc-functionalized intermediate **1**. The characteristic peak at 4.00 ppm for internal CH<sub>2</sub> protons of G4-OH in NMR confirmed the formation of an ester bond with the linker. A multiplet at 1.72 ppm for GABA linker CH<sub>2</sub> protons and multiplets between 7.30 and 7.86 for aromatic Fmoc protons confirmed the formation of the bond. We calculated the loading of the linker by comparing the amidic protons of the dendrimer with aliphatic CH<sub>2</sub> protons of the linker, which suggested that in each batch we had 40–45 molecules attached to each dendrimer. This number was consistent in each of three large batches. Without further purifying the intermediate, we carried out the

deprotection step with piperidine (20% in DMF) to get free amine-functionalized dendrimers (**2**). Absence of Fmoc aromatic proton peaks in NMR confirmed the deprotection of Fmoc groups. Using the proton integration method, we calculated the number of linkers attached to each dendrimer. In each case, results indicated 21–24 NH<sub>2</sub> groups on the surface of each dendrimer. This may differ from the calculated loading due to hydrolysis of the ester bond under basic conditions (piperidine), water content in DMF, and the dialysis at room temperature for 24 to 30 h.

**Preparation PEG-Valproic Acid (PEG-VPA).** Valproic acid was functionalized with a thiol-reactive group, which was further reacted with the dendrimer. We reacted a short PEG-SH having three repeating units of (CH<sub>2</sub>)<sub>2</sub>O— with valproic acid using DCC as coupling reagent as shown in Figure 3B. The crude PEG-VPA obtained was purified by column chromatography and characterized by proton NMR. In the NMR spectrum, there was a down-shift of the peak of CH<sub>2</sub> protons neighboring to OH group of PEG to 4.25 ppm from 3.65 ppm that confirmed the formation of PEG-VPA (Figure S5). Although the thiol group also may be susceptible to reacting with acid functionality, the NMR spectra did not indicate any downward shift of the peak belonging to CH<sub>2</sub> protons adjacent to thiol group of PEG. This suggested that the thiol group was free to react with the thiol-reactive functionalized dendrimer.

**Preparation of Dendrimer-PEG-Valproic Acid Conjugate (D-VPA, **4**).** We designed a D-VPA conjugate, which would enable intracellular glutathione-triggered VPA

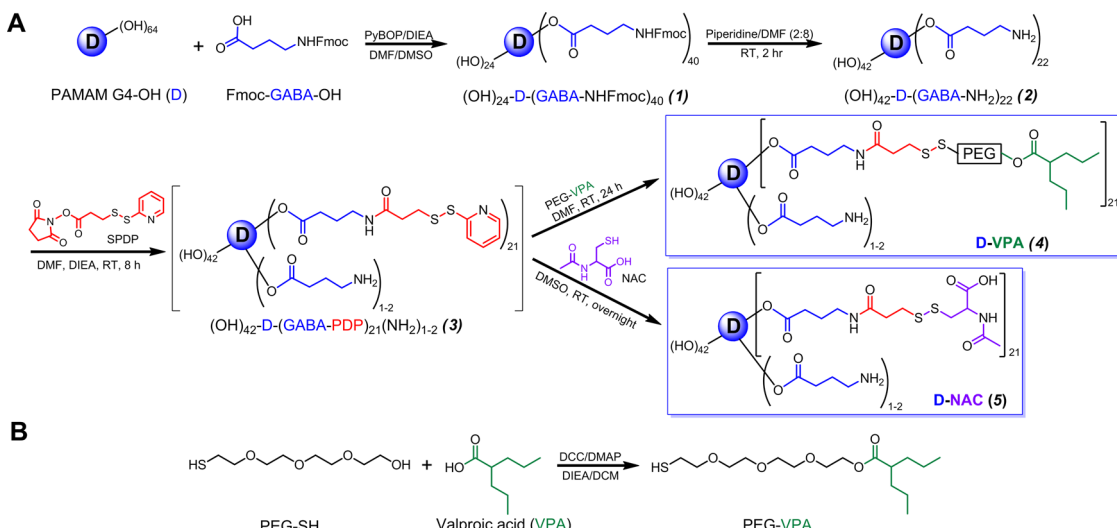


**Figure 3.** (A) Schematic presentation of the preparation of bifunctional dendrimer (2), dendrimer-PEG-valproic acid (D-VPA, 4), and dendrimer-N-acetylcysteine (D-NAC, 5). (B) Preparation of thiol-functionalized PEG-valproic acid (PEG-VPA).

release, by having a disulfide bond between dendrimer and valproic acid (Figure 3). This was a two-step process after the synthesis of bifunctional dendrimer; the first step was the reaction of amine-functionalized dendrimer with *N*-succinimidyl-3-(2-pyridyl)dithiopropionate (SPDP), and the second one involved thiol-functionalized valproic acid. SPDP was reacted with the intermediate **2** in the presence of DIEA to obtain pyridylidithio (PDP)-functionalized dendrimer **3**. Even though this was an *in situ* reaction process, we established the structure by <sup>1</sup>H NMR. In the spectrum, new peaks between 6.7 and 7.6 ppm for aromatic protons of pyridyl groups confirmed the formation of the product. We verified the number of pyridyl groups and number of GABA linkers to be the same, which indicated that most of the amine groups reacted with the SPDP. Since this was a key step for the conjugation of the drug to the dendrimer, we validated the use of mole equivalents of SPDP per amine group and time required for the reaction. Finally, the PEG-VPA was reacted with the PDP-functionalized dendrimer *in situ* to get dendrimer-PEG-valproic acid (D-VPA, **4**). The formation of the final conjugate and loading of VPA were confirmed by <sup>1</sup>H NMR, and the purity of the conjugate was evaluated by reverse-phase HPLC. In the NMR spectrum, multiplets between 0.85 and 1.67 ppm for aliphatic protons of VPA, multiplets between 3.53 and 3.66 ppm for CH<sub>2</sub> protons of PEG, and absence of pyridyl aromatic protons confirmed the conjugate formation (Figure S6). We estimated the loading of the VPA (~21 molecules) using a proton integration method, which suggested that 1–2 amine groups were left unreacted. In the HPLC chart, the elution time of D-VPA (17.2 min) was different from that for G4-OH (9.5 min), confirming that the conjugate was pure, with no measurable traces of VPA (23.4 min) and PEG-VPA (39.2 min) (Figure 4). The percentage of VPA loading to the dendrimer

was ~12% w/w and validated the method for making gram quantities in three different batches.

**Preparation of Dendrimer-NAC Conjugate (D-NAC, 5).** We previously described the preparation of D-NAC for therapy in a rabbit model of perinatal brain injury, where the conjugate was prepared in 100 mg quantities.<sup>23</sup> Here, we report a more efficient scheme, with better yield, and large-scale, multigram synthesis of D-NAC (Figure 3A). We established the formation of the intermediate **3**, which is the key precursor for the synthesis of both D-VPA and D-NAC. Finally, *N*-acetylcysteine was reacted with intermediate **3** overnight to get D-NAC with disulfide linkage. In the <sup>1</sup>H NMR spectrum, a multiplet at 1.65 ppm for CH<sub>2</sub> protons of the linker, a singlet at 1.85 ppm for acetyl protons of NAC, and a multiplet at 4.35–4.48 for CH protons of NAC confirmed the product formation (Figure S7). We calculated the loading of NAC to the dendrimer using a proton integration method. Since ~21 PDP groups were present on the surface, 21 NAC molecules were reacted to the dendrimer and the drug loading was ~16 wt %. In the HPLC chromatogram, the D-NAC conjugate eluted at 23.5 min, whereas the retention times of free NAC (4.5 min) and dendrimer (19.9 min) were different (Figure 4B). No detectable amount of free NAC was present in the conjugates, suggesting that the conjugate is comparatively pure and soluble in water, saline, and PBS buffer. These results suggest that we were able to prepare multigram scale quantities of D-NAC and the intermediates reproducibly.

**Dendrimer–Drug Conjugates Are Associated with Decreased Systemic Side Effects and Improved Neurological Outcomes Compared to Free Drugs at 10-Fold (VPA) and 30-Fold (NAC) Higher Doses.** Treatment with high doses of free NAC and free VPA is associated with significant side effects such as peri-operative hypotension requiring fluid resuscitation and inotropic support, pulmonary edema/hemorrhage, and difficulty in cardioversion to

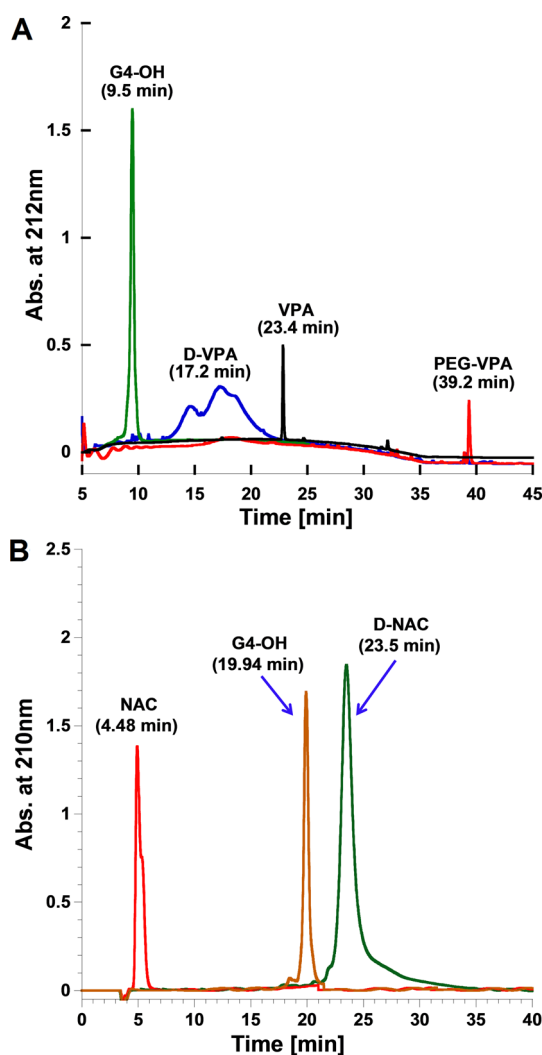


**Figure 4.** (A) HPLC chromatogram of dendrimer-VPA (D-VPA, 17.2 min), valproic acid (VPA, 23.4 min), and PEG-VPA (39.2 min) monitored at 212 nm in PDA detector. (B) HPLC chart of dendrimer-*N*-acetylcysteine (D-NAC, 23.5 min), dendrimer (G4-OH, 19.9 min), and NAC (4.48 min).

a sinus rhythm. Circulatory arrest and hypothermia are known to result in decreased drug clearance, increased serum drug levels, and altered drug responses.<sup>19</sup> Hence adverse effects of drugs and toxicity of drugs may often be exaggerated in the context of HCA. Pilot studies investigated free VPA, free NAC, free VPA combined with free NAC, D-NAC, and a combination of D-NAC + D-VPA. Dogs undergoing 2 h HCA were treated with one of the following: (1) vehicle (saline,  $n = 5$ ), (2) free VPA at 100 mg/kg ( $n = 5$ ), (3) free NAC at 300 mg/kg ( $n = 2$ ), (4) VPA (100 mg/kg) + NAC (300 mg/kg) ( $n = 5$ ), (5) D-NAC at 3 mg/kg NAC in 15 mg/kg of dendrimer ( $n = 1$ ), or (6) D-VPA + D-NAC containing 10 mg/kg of VPA in 70 mg/kg of dendrimer (12% payload) and 10 mg/kg of NAC in 50 mg/kg of dendrimer (16% payload) ( $n = 1$ ). Results for all animals that survived beyond 24 h are reported.

Biosafety of the vehicle hydroxyl G4-OH dendrimer used in this study, following systemic administration

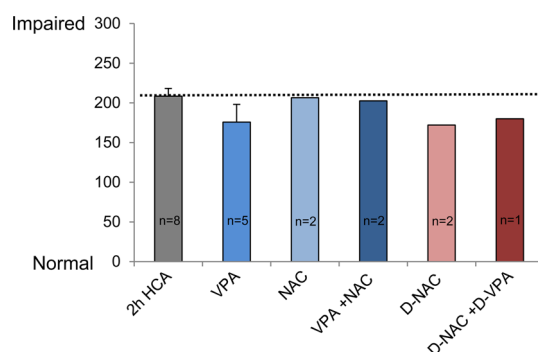


**Figure 5.** Neurobehavioral scores 24 h after HCA. Neurological deficits were scored in a recent set of vehicle-treated dogs 24 h after HCA and in initial studies of free VPA (100 mg/kg), free NAC (300 mg/kg), free NAC (300 mg/kg) + free VPA (100 mg/kg), D-NAC (3 mg/kg), or D-NAC + D-VPA (10 mg/kg each). On this scoring scale, 300 corresponds to a highly impaired animal, and 0 corresponds to normal.

on day 1 (~5-fold higher than the levels used in this study), was evaluated in healthy newborn rabbit kits at day 5 and day 15 of age. There was no change in renal and hepatic functions or neurobehavior noted at both time points when compared to healthy kits administered PBS.<sup>23</sup> Histopathological evaluation of the major organs (brain, kidney, liver, lung, heart, spleen) on day 5 and day 15 demonstrated normal architecture, without cellular loss or neutrophil infiltration. D-Cy5 imaging and quantification suggested that the dendrimer was mostly cleared intact with 24–48 h.<sup>54</sup> Our studies are consistent with those of recent extensive toxicity studies in mouse models, which suggested that hydroxyl PAMAM dendrimers are noncytotoxic up to 550 mg/kg and do not cause protein opsonization or blood hemolysis.<sup>57,58</sup>

**Neurological Assessment.** Neurological deficits were scored 24 h after HCA in prior studies of vehicle- or VPA (100 mg/kg)-treated dogs and in pilot studies of NAC (300 mg/kg), NAC (300 mg/kg) + free VPA (100 mg/kg), D-NAC (3 mg/kg) or D-NAC (10 mg/kg) + D-VPA (10 mg/kg). Only two of the three dogs in the VPA + NAC group survived to 24 h for neurologic assessment. The dog that died had severe hemodynamic complications due to hypotension and acidosis (Figure 5). We previously showed that free VPA (100 mg/kg) improved neurological deficit scores at 24 h but was associated with hypotension and pulmonary complications (edema and hemorrhage).<sup>13</sup> Free NAC at 300 mg/kg and combination therapy with free VPA (100 mg/kg) + free NAC (300 mg/kg) did not lead to improvements in neurological deficit scores at 24 h (Figure 5). D-NAC at low doses (3 mg/kg) improved neurological scores after 24 h, but it was not sustained at 72 h (neurological deficit score comparable to untreated controls), suggesting that higher doses may be better. Combination therapy with D-NAC (10 mg/kg) + D-VPA (10 mg/kg) improved neurological scores at 24 h (Figure 5), and the improvement was comparable to that achieved with free VPA treatments at 100 mg/kg.

The improvement in neurological deficit score following D-NAC + D-VPA combination therapy was somewhat better than that achieved with free drug combination therapy at 30-fold (NAC) and 10-fold (VPA) higher doses. Since the number of animals was not large enough for detailed statistical analysis, the dendrimer–drug groups were combined together (D-NAC and D-NAC + D-VPA ( $n = 3$ ; mean deficit score = 174) and compared with vehicle-treated groups ( $n = 8$ ; mean deficit score = 208) using a *t* test. The analysis suggested a trend of improvement ( $p = 0.085$ ) with reduced deficit scores in dendrimer–drug treated animals.

We chose the doses for free and dendrimer–drug conjugates based on prior studies. We have performed extensive studies on free NAC versus dendrimer-NAC in a rabbit model of cerebral palsy<sup>23</sup> and free VPA in this canine model.<sup>13</sup> To understand how the dendrimer may improve the drug delivery to the brain, it may be important to measure drug levels with and without dendrimer. It is challenging to measure NAC and VPA levels in the brain, and this would provide only gross levels, not the selective targeting of injured cells. In a preliminary experiment, we measured the serum ( $\sim 150 \mu\text{g/mL}$ ) and CSF ( $\sim 40 \mu\text{g/mL}$ ) levels of free VPA (2 h after IV administration of 100 mg/kg as used in the therapy studies above). These CSF and serum levels compare well with those reported previously in canine and small animal models.<sup>59–61</sup> We compared this to the dendrimer serum (35  $\mu\text{g/mL}$ ) and CSF (0.25  $\mu\text{g/mL}$ ) levels (2 h after IV administration of 5 mg/kg of D-FITC as in the biodistribution studies above, Figure 3). Since the dendrimer was administered at a much lower level (20-fold), on an equal mass basis, the dendrimer would have a higher serum level but lower CSF level compared to free VPA. Clearly, the CSF/serum ratio of free VPA is much higher than that of the dendrimer, yet the dendrimer-conjugated drugs show comparable efficacy at a significantly lower dose. This may be attributable to selective delivery to injured cells, reduced protein binding of conjugated drugs, and reduced side effects.

**Adverse Side Effects during HCA.** Treatment with high doses of free NAC and free VPA are associated with significant side effects, such as peri-operative hypotension requiring fluid resuscitation and inotropic support, pulmonary edema/hemorrhage, and difficulty in cardioversion to a sinus rhythm. Circulatory arrest and hypothermia are known to result in decreased drug clearance, increased serum drug levels, and altered drug responses.<sup>19</sup> Hence, adverse effects of drugs and toxicity of drugs are likely to be exaggerated in the context of HCA. These were evaluated by assessing the hemodynamic support required during HCA. Free VPA (100 mg/kg), free NAC (300 mg/kg), and NAC + VPA exacerbated the adverse effects, requiring increased hemodynamic support compared to vehicle-treated animals (Figure 6). Animals that received free VPA or NAC at doses in the range needed to provide

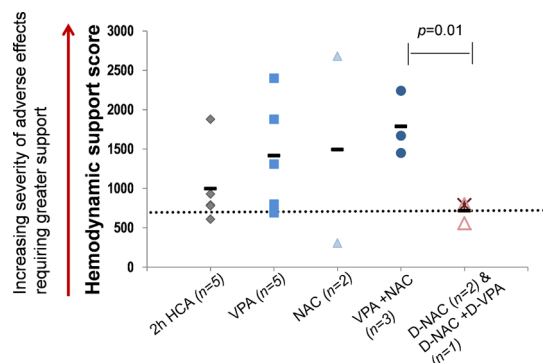


**Figure 6. Hemodynamic support provided during HCA.** Hemodynamic support scores for each dog in the different treatment groups is shown with the mean score for each group indicated by the dark line. The doses used are the same as those used in the neurological deficit studies in Figure 5. An increase in hemodynamic adverse effects was observed during and after rewarming in animals given free VPA, free NAC, or combined free drug therapy. In contrast, dendrimer-linked drugs required less hemodynamic support and were similar to untreated animals subjected to HCA. Dogs that received VPA + NAC therapy had significantly higher hemodynamic support scores (more adverse effects) when compared to dogs that received the dendrimer–drug conjugates (D-NAC alone indicated by triangles, and D-NAC+D-VPA indicated by a X) ( $p = 0.01$ ).

neuroprotection consistently had major adverse effects related to hypotension and metabolic acidosis and required several attempts at cardioversion. This is similar to adverse effects seen in patients, which included significant metabolic acidosis and hypotension when administered VPA after complex aortic surgery (unpublished data). These adverse effects were not seen in the dogs that received D-NAC or D-NAC + D-VPA. Dogs that received free VPA + NAC therapy had significantly higher hemodynamic support scores (more adverse effects) when compared to dogs that received the dendrimer–drug conjugates ( $p = 0.01$ ). The dendrimer conjugates produced neurological improvements comparable to free VPA, but at 10–30-fold lower doses, with fewer adverse effects. The dendrimer conjugates also had lower mean hemodynamic scores compared to the free VPA or free NAC groups, but statistical significance was not analyzed, due to the small number of animals in the free NAC and dendrimer groups and the relatively large variability in the hemodynamic support required for the free VPA group. The reduced adverse effects associated with the dendrimer–drug conjugates may be due to lower doses required to achieve neuroprotection in these animals since the dendrimer may be delivering the drugs to injured neurons and microglia. Moreover, since the dendrimer has a relatively short circulation time, remains intact due to low GSH levels in plasma,<sup>23,56</sup> and is rapidly excreted in the urine, dendrimer–drug conjugates that are not taken up by activated microglia or injured neurons in the brain will likely be excreted intact in the urine. The dendrimer conjugate is expected to release

most of the drug intracellularly, where glutathione concentrations are much higher, facilitating its action on the thiol linker and leading to release of the drug. This will also result in less free drug in circulation, which may reduce systemic side effects.

## CONCLUSIONS

Although large animal models have several limitations, especially related to costs, managing cardiac surgical procedures, and the need for large-scale preparation of dendrimer–drug conjugates, this canine model captures many important features of brain injury following HCA as it occurs in humans and may thus facilitate faster translation to clinical practice if therapies are successful.<sup>13,14</sup> While small animal models are essential to gaining insights into the molecular and cellular basis of cardiovascular biology, significant differences exist with regard to cardiac characteristics such as heart rate, oxygen consumption, adrenergic receptor ratios, and contractile protein expression. Thus, it becomes difficult to make interpretations of human pathophysiology based on extrapolations of murine systems, especially after the induction of cardiovascular stress. Large animal models like canines, which more closely approximate human physiology, anatomy, and function, are therefore essential components in the translation of clinical therapies from bench to bedside.<sup>13,62</sup>

Neuroinflammation may be an emerging opportunity for nanomedicine. Building on results that show the ability of PAMAM dendrimers to selectively localize in microglia in small animal models,<sup>23–25</sup> we performed PAMAM dendrimer brain uptake and efficacy studies for the first time in a large animal model of HCA-associated brain injury. Fluorescence labeling enabled biodistribution, quantification and brain uptake imaging. These hydroxyl-terminated PAMAM dendrimers appeared to cross the injured blood-brain barrier and localize in injured hippocampal dentate granule cells and cerebellar Purkinje and granule cells and microglia. The uptake and retention of the dendrimer in the brain was quantifiable. Even though the brain uptake of dendrimer, 6 h after administration, appears low (~0.02% of the injected dose), it is significantly higher than free NAC levels (as a percentage of injected dose) reported in the brain of small animals.<sup>63</sup> In addition, the selective localization of the dendrimer in injured cells may enable improved drug delivery. We showed that a similar extent of dendrimer uptake in the brain produced significant efficacies in a rabbit model of cerebral palsy.<sup>23</sup> The biodistribution of the dendrimer in other major organs was qualitatively

similar to what is seen in small animal models.<sup>46–49</sup> The CSF/serum ratio was ~1% over the first 24 h. We demonstrated that it is feasible to produce large quantities of D-NAC and D-VPA in a standardized manner for efficacy studies in this large animal model. In preliminary efficacy studies, we showed that the dendrimer–drug conjugates were as effective as the free drug alone or in combination, but at a much lower dose, in improving neurobehavioral outcomes. Moreover, administration of the dendrimer–drug conjugates was not associated with as many adverse hemodynamic effects as free drug administration.

Toxic effects have been noted from free drugs administered after cardiac arrest and bypass at doses that are commonly used clinically.<sup>19–21</sup> This may occur due to alterations in drug clearance, drug metabolism, and drug–receptor binding. Based on these preliminary results and our previous data using VPA, it appears that this dose of VPA and NAC is required to achieve neuroprotection. However, the severe systemic side effects associated with these doses will limit clinical translation. This can be overcome by use of dendrimer–drug conjugates at much lower doses. Since the dendrimers can cross the impaired blood-brain barrier and localize selectively in injured cells, we speculate that they may provide neuroprotection at a much lower dose. Since the drug is mainly released intracellularly and the circulation time for the dendrimer is low, most of the dendrimer–drug conjugate that is not taken up by cells is excreted intact by the kidneys. This prevents systemic side effects on the cardiovascular system that are associated with the free drug. Moreover, since the standard routes for drug metabolism and clearance are bypassed due to the use of the dendrimer–drug delivery system, the risk of increased accumulation of the drug resulting in toxicity following cardiac arrest is decreased.

Even though the efficacy studies are preliminary, with dendrimer–drug conjugates studied in a small number of animals, we focused on demonstrating the brain uptake of dendrimers and the therapeutic feasibility of this approach and on the reduction in adverse systemic side effects. The “best” improvement in neurological outcomes with free drugs, or their combination, was achieved for free VPA at 100 mg/kg. The dendrimer conjugates produced comparable improvements in neurological outcomes at 1/10th the dose and were accompanied by reduced drug side effects. The results are encouraging and support the need for further studies to determine dose responses for the free drugs and dendrimer–drug conjugates and to demonstrate the effectiveness of this approach in this large animal model.

## MATERIALS AND METHODS

**Materials and Characterization of the Conjugates.** The details relating to materials and reagents used for the synthesis of

dendrimer–drug conjugates (D-VPA and D-NAC, and the methods for characterization of the resultant nanodevices (<sup>1</sup>H NMR, HPLC, etc.) have been described in the Supporting Information.

Generation-4, primary hydroxyl-functionalized PAMAM dendrimers (molecular weight  $\approx$ 14 200 Da) with ethylenediamine (EDA) core were used in these studies.

**Preparation of the Conjugates.** Detailed synthetic procedure of bifunctional dendrimer [(OH)<sub>42</sub>-D-(GABA-NH<sub>2</sub>)<sub>22</sub>, **2**] and the final conjugate dendrimer-*N*-acetylcysteine (D-NAC, **5**) are described in Supporting Information.

**Synthesis of SH-PEG-Valproic Acid (PEG-VPA).** To a stirred solution of valproic acid (2.18 g, 15.16 mmol) in dichloromethane (50 mL) were added DCC (4.68 g, 22.74 mmol) dissolved in anhydrous DCM (60 mL) and DMAP (720 mg) under nitrogen. The reaction mixture was cooled to 0 °C, and DIEA (3.4 mL) was added to it and stirred for 30 min. Finally, the thiol-PEG3-alcohol (PEG-SH; 1.40 g, 8.42 mmol) dissolved in anhydrous DCM (20 mL) was added to the reaction and stirred overnight at room temperature. The reaction was monitored by thin layer chromatography. The byproduct was filtered, and the solvent was evaporated under reduced pressure. The crude was purified by column chromatography using 25% ethyl acetate in hexane to get the desired PEG-VPA (1.75 g, yield: 70%). <sup>1</sup>H NMR ( $\text{CDCl}_3$ ):  $\delta$  0.89–0.92 (t, 6H,  $\text{CH}_3$  of VPA), 1.26–1.33 (m, 4H,  $\text{CH}_2$  of VPA), 1.41–1.45 (m, 2H,  $\text{CH}_2$  of VPA), 1.58–1.63 (m, 2H,  $\text{CH}_2$  of VPA), 2.38–2.43 (m, 1H, CH of VPA), 2.88–2.91 (t, 2H, SH– $\text{CH}_2$  of PEG), 3.63–3.76 (m, 8H,  $\text{OCH}_2$  of PEG), 4.24–4.26 (t, 2H,  $\text{OCOCH}_2$  of PEG).

**Synthesis of Dendrimer-PEG-Valproic Acid Conjugate (D-VPA, **4**).** Amine-functionalized dendrimer **2** (4.32 g, 0.269 mmol) was dissolved in anhydrous DMF (200 mL), and DIEA (2.6 mL) was added to it. The reaction mixture was cooled to 0 °C, and SPDP (2.82 g, 9.04 mmol) dissolved in anhydrous DMF (100 mL) was added slowly by maintaining the temperature of the reaction mixture for 30 min. The reaction mixture was allowed to stir at room temperature overnight, and again SPDP (1.87 g, 5.99 mmol) dissolved in DMF (70 mL) was added and stirred for 8 h. Finally, PEG-VPA (1.75 g, 5.99 mmol) dissolved in DMF (50 mL) was added to the reaction mixture and stirred for 24 h. The solvent was evaporated under reduced pressure, and the obtained crude product was dialyzed in DMF using dialysis membrane (MWCO; 1 kDa) for 24 h. Finally, the solvent was evaporated, and the product was reconstituted with PBS buffer (pH 7.4) and dialyzed against water for 6–8 h. The water was lyophilized to get D-VPA conjugate (4.18 g). <sup>1</sup>H NMR ( $\text{DMSO}-d_6$ ):  $\delta$  0.85–0.87 (t,  $\text{CH}_3$  protons, VPA), 1.21–1.27 (m,  $\text{CH}_2$  protons, VPA), 1.36–1.42 (m,  $\text{CH}_2$  protons, VPA), 1.47–1.50 (m,  $\text{CH}_2$  protons, VPA), 1.64–1.67 (t,  $\text{CH}_2$  protons, linker), 2.26–2.37 (m,  $\text{CH}_2$  protons of G4-OH, CH protons of VPA, linker protons), 2.43–3.42 (m,  $\text{CH}_2$  protons of G4-OH, SS– $\text{CH}_2$  of PEG,  $\text{CH}_2$  of SPDP), 3.53–3.66 (m,  $\text{OCH}_2$  backbone protons of PEG), 4.02 (br s,  $\text{CH}_2\text{OC}=\text{O}$  protons, G4-OH), 4.14–4.16 (t,  $\text{OCOCH}_2$  protons, PEG), 7.84–8.13 (m, NHCO protons of G4-OH and linker).

**Canine HCA Model and Experimental Design.** All experiments used a canine model of HCA developed in by the Baumgartner laboratory.<sup>26,27</sup> This large animal model takes advantage of certain inherent physiologic similarities between humans and canines to develop a readily translatable therapeutic model to address the neurologic injury associated with hypothermic circulatory arrest. Because this is a large animal model, we are able to replicate surgical procedures with impressive fidelity to that experienced in human operating rooms and are able to replicate a degree of neurologic injury similar to that seen in the worst human cases. However, due to the large animal protocol, ethical requirement to minimize animal numbers and the expense required to maintain such a program, we are unable to readily produce the number of experiments that may be seen in small animal models such as mice and rats. Therefore, we endeavored to establish therapeutic efficacy with the minimum number of experiments necessary and then expand upon these findings with further biochemical and genetic analyses.

Conditioned, heartworm-negative, 6–12 month old, male, class-A dogs (approximately 30 kg) were used for all experiments (Marshal Bioresources, North Rose, NY). Experiments were approved by The Johns Hopkins University School of Medicine Animal Care and Use Committee and complied with the "Guide for the Care and Use of Laboratory Animals" (1996, U.S. National Institutes of Health).

Dogs were administered methohexitol sodium (12 mg/kg IV, in divided doses), endotracheally intubated, and maintained on

isoflurane inhalational anesthesia (0.5–2.0%), 100% oxygen, and IV fentanyl (150–200  $\mu\text{g}/\text{dose}$ ), and midazolam (2.5 mg/dose). Tympanic membrane, esophageal, and rectal probes monitored temperatures throughout the experiment. A left femoral artery cannula was placed prior to the initiation of CPB for monitoring blood pressure and sampling of arterial blood gases. EKG was continuously monitored. As previously described, the right femoral artery was cannulated and the cannula advanced into the descending thoracic aorta. Venous cannulae were advanced to the right atrium from the right femoral and right external jugular veins. Closed-chest CPB was initiated, and the animals were cooled. Pump flows of 60–100 mL/kg/min maintained a mean arterial pressure of 60–80 mmHg. Once tympanic temperatures reached 18 °C, the pump was stopped and blood was drained by gravity into the reservoir. Dogs underwent 2 h HCA with standard hemodilution and alpha-stat regulation of arterial blood gases. After HCA, CPB was restarted and the animals were rewarmed to a core temperature of 37 °C over the course of 2 h. If sinus rhythm did not return spontaneously, the heart was defibrillated at 32 °C. Serial blood gas levels were taken to ensure adequate pH and verify electrolyte concentrations, and continuous hemodynamic measurements were recorded utilizing an arterial cannula. At 37 °C, each dog was weaned from CPB and the cannulae were removed. Dogs recovered from anesthesia while intubated, with frequent monitoring of vital signs, arterial blood gases, and urine output. Some animals required hemodynamic support and correction of acidosis at this stage to enable successful weaning from bypass. Once hemodynamically and clinically stable, dogs were extubated and transferred to their cages for recovery and survival, with neurologic assessments at 24 h intervals until the desired end point (24 or 72 h after bypass).

**Dendrimer Administration (for Biodistribution Studies).** Dendrimer–fluorophore conjugates were injected as a one-time bolus 24 h after hypothermic circulatory arrest. Three dogs were concurrently treated with intravenous infusion of D-FITC (140 mg per animal,  $\sim$ 5 mg/kg) and intracisterna magna (ICM, "into the brain") injection of D-Cy5 (5 mg per animal, 0.17 mg/kg) and euthanized 48 h post-conjugate administration. Tissue uptake and biodistribution were subsequently measured at sacrifice (48 h after administration). Since FITC and Cy5 were analyzed at their distinct characteristic wavelengths, their biodistribution could be assessed simultaneously.

**Dendrimer Administration (for Efficacy Studies).** Free drugs (VPA and NAC) or dendrimer–drug conjugates were administered intravenously before and after HCA. Doses for free drug administration were based on our previous studies in which neuroprotection was achieved with free VPA and based on the literature for free *N*-acetylcysteine. Previous studies have reported that pretreatment with NAC is protective in models of cardiac arrest. Doses for the dendrimer–drug conjugates were set at 1/10 (VPA) or 1/30 (NAC) of the free drug doses, based on our prior findings of striking neuroprotection at such dose ratios in the rabbit CP model.<sup>23</sup> Therefore, for the free drugs, animals were treated with 100 mg/kg of VPA and 300 mg/kg of NAC, of which half the dose was administered intravenously prearrest and the rest was administered postarrest. For the dendrimer–drug conjugates, dogs were treated intravenously with D-NAC containing 10 mg/kg of NAC and/or D-VPA with 10 mg/kg of VPA. D-VPA was administered intravenously as a 25% bolus prior to HCA, followed by 75% infusion over 2 h after HCA was completed. D-NAC was intravenously administered as a 50% bolus pre-HCA and a 50% infusion over 2 h after HCA was complete. These regimens are similar to what was used for free drugs.

**Euthanasia.** Animals were euthanized by exsanguination. After sedation and intubation, animals underwent median sternotomy and cannulation of the ascending aorta using a 22-French cannula. CPB was initiated after clamping the descending aorta to ensure the brain was perfused with 12 L of ice-cold saline (4 °C) at 60 mmHg. The right atrial appendage was transected, and the venous return was allowed to drain. Brains were harvested immediately after perfusion, hemispheres were separated, and one hemisphere was fixed in 10% neutral buffered formalin (for immunohistochemical evaluation and

imaging) while the other hemisphere was cut into 1 cm coronal slices and rapidly frozen (for biodistribution quantification).

**Fluorescence Microscopy.** Cryostat sections of hippocampus and cerebellum were mounted with antifade media (Prolong Gold with DAPI, Molecular Probes, Inc., Eugene, OR). Fluorescence images were obtained using a Zeiss AxioImager M2, with equal exposure times for all samples of each brain region. To optimize image contrast and brightness, display settings were adjusted equally within each set of images.

**Hemodynamic Support Score.** A hemodynamic support score was calculated for all animals based on the amount of inotropic support, fluid boluses administered to maintain normal hemodynamic status, and the number of attempts at cardioversion required to achieve a sinus rhythm. This was based on modification of vasoactive inotropic scores used for evaluating outcomes following congenital cardiac repairs.<sup>64,65</sup> The hemodynamic support score is calculated as the vasoactive inotropic score + fluid resuscitation score + cardioversion score = (phenylephrine (mg) × 100 + epinephrine (mg) × 100) + (IV fluid (L) above 1L (maintenance fluids) × 100) + (number of attempts at cardioversion × 100). This score is dependent on the degree of hypotension and the underlying cardiac function. A greater score indicates a greater need for hemodynamic support.

**Neurologic Evaluation.** Clinical neurologic assessment was performed on all animals every 24 h until sacrifice. The dog-specific behavior scale used in this study was validated at the International Resuscitation and Research Center, University of Pittsburgh School of Medicine.<sup>66</sup> There were five components of neurologic function evaluated: level of consciousness, respiratory pattern, cranial nerve function, motor and sensory function, and behavior. Two investigators independently assigned each component a score between 0 (normal) and 100 (severe injury), and these were averaged and summed to obtain the total score, with a possible range from 0 (normal) to 500 (brain death).

**Conflict of Interest:** The authors declare no competing financial interest.

**Acknowledgment.** This study was supported by the National Institutes of Health (NIH RO1 HL091541-18, W.A.B.). The authors would like to thank Ms. Jennifer Berrong for brain tissue preparation. We also express profound gratitude to Mr. Jeffrey Brawn and Mrs. Melissa Jones for their invaluable technical assistance and support. Their decades-long experience with the experimental protocol was vital to completion of this study.

**Supporting Information Available:** Detailed synthesis and characterization of dendrimer-Cy5 (D-Cy5) and dendrimer-NAC (D-NAC), and sample preparation and quantification of D-FITC and D-Cy5 in biological specimens. This material is available free of charge via the Internet at <http://pubs.acs.org>.

## REFERENCES AND NOTES

- Selnes, O. A.; Gottesman, R. F.; Grega, M. A.; Baumgartner, W. A.; Zeger, S. L.; McKhann, G. M. Cognitive and Neurologic Outcomes after Coronary-Artery Bypass Surgery. *N. Engl. J. Med.* **2012**, *366*, 250–257.
- Tarakji, K. G.; Sabik, J. F., III; Bhudia, S. K.; Batizy, L. H.; Blackstone, E. H. Temporal Onset, Risk Factors, and Outcomes Associated with Stroke after Coronary Artery Bypass Grafting. *JAMA* **2011**, *305*, 381–390.
- Roach, G. W.; Kanchuger, M.; Mangano, C. M.; Newman, M.; Nussmeier, N.; Wolman, R.; Aggarwal, A.; Marschall, K.; Graham, S. H.; Ley, C. Adverse Cerebral Outcomes after Coronary Bypass Surgery. Multicenter Study of Perioperative Ischemia Research Group and the Ischemia Research and Education Foundation Investigators. *N. Engl. J. Med.* **1996**, *335*, 1857–1863.
- Newman, M. F.; Kirchner, J. L.; Phillips-Bute, B.; Gaver, V.; Grocott, H.; Jones, R. H.; Mark, D. B.; Reves, J. G.; Blumenthal, J. A. Longitudinal Assessment of Neurocognitive Function after Coronary-Artery Bypass Surgery. *N. Engl. J. Med.* **2001**, *344*, 395–402.
- Augoustides, J. G.; Floyd, T. F.; McGarvey, M. L.; Ochroch, E. A.; Pochettino, A.; Fulford, S.; Gambone, A. J.; Weiner, J.; Raman, S.; Savino, J. S.; et al. Major Clinical Outcomes in Adults Undergoing Thoracic Aortic Surgery Requiring Deep Hypothermic Circulatory Arrest: Quantification of Organ-Based Perioperative Outcome and Detection of Opportunities for Perioperative Intervention. *J. Cardi thorac. Vasc. Anesth.* **2005**, *19*, 446–452.
- Newburger, J. W.; Jonas, R. A.; Wernovsky, G.; Wypij, D.; Hickey, P. R.; Kuban, K. C.; Farrell, D. M.; Holmes, G. L.; Helmers, S. L.; Constantinou, J.; et al. A Comparison of the Perioperative Neurologic Effects of Hypothermic Circulatory Arrest versus Low-Flow Cardiopulmonary Bypass in Infant Heart Surgery. *N. Engl. J. Med.* **1993**, *329*, 1057–1064.
- Bigelow, W. G.; Lindsay, W. K.; Greenwood, W. F. Hypothermia; Its Possible Role in Cardiac Surgery: An Investigation of Factors Governing Survival in Dogs at Low Body Temperatures. *Ann. Surg.* **1950**, *132*, 849–866.
- Di Eusanio, M.; Schepens, M. A.; Morshuis, W. J.; Dossche, K. M.; Di Bartolomeo, R.; Pacini, D.; Pierangeli, A.; Kazui, T.; Ohkura, K.; Washiyama, N. Brain Protection Using Antegrade Selective Cerebral Perfusion: A Multicenter Study. *Ann. Thorac. Surg.* **2003**, *76*, 1181–1188 discussion 1188–1189.
- Lytle, B. W.; McCarthy, P. M.; Meaney, K. M.; Stewart, R. W.; Cosgrove, D. M., III. Systemic Hypothermia and Circulatory Arrest Combined with Arterial Perfusion of the Superior Vena Cava. Effective Intraoperative Cerebral Protection. *J. Thorac. Cardiovasc. Surg.* **1995**, *109*, 738–743.
- Drew, C. E.; Anderson, I. M. Profound Hypothermia in Cardiac Surgery: Report of Three Cases. *Lancet* **1959**, *1*, 748–750.
- Bellinger, D. C.; Jonas, R. A.; Rappaport, L. A.; Wypij, D.; Wernovsky, G.; Kuban, K. C.; Barnes, P. D.; Holmes, G. L.; Hickey, P. R.; Strand, R. D.; et al. Developmental and Neurologic Status of Children after Heart Surgery with Hypothermic Circulatory Arrest or Low-Flow Cardiopulmonary Bypass. *N. Engl. J. Med.* **1995**, *332*, 549–555.
- Hickey, P. R. Neurologic Sequelae Associated with Deep Hypothermic Circulatory Arrest. *Ann. Thorac. Surg.* **1998**, *65*, S65–69 discussion S69–70, S74–6.
- Williams, J. A.; Barreiro, C. J.; Nwakanma, L. U.; Lange, M. S.; Kratz, L. E.; Blue, M. E.; Berrong, J.; Patel, N. D.; Gott, V. L.; Troncoso, J. C.; et al. Valproic Acid Prevents Brain Injury in a Canine Model of Hypothermic Circulatory Arrest: A Promising New Approach to Neuroprotection during Cardiac Surgery. *Ann. Thorac. Surg.* **2006**, *81*, 2235–2241 discussion 2241–2242.
- Barreiro, C. J.; Williams, J. A.; Fitton, T. P.; Lange, M. S.; Blue, M. E.; Kratz, L.; Barker, P. B.; Degaonkar, M.; Gott, V. L.; Troncoso, J. C.; et al. Noninvasive Assessment of Brain Injury in a Canine Model of Hypothermic Circulatory Arrest Using Magnetic Resonance Spectroscopy. *Ann. Thorac. Surg.* **2006**, *81*, 1593–1598.
- Louwerse, E. S.; Weverling, G. J.; Bossuyt, P. M.; Meyjes, F. E.; de Jong, J. M. Randomized, Double-Blind, Controlled Trial of Acetylcysteine in Amyotrophic Lateral Sclerosis. *Arch. Neurol.* **1995**, *52*, 559–564.
- Ferrari, G.; Yan, C. Y.; Greene, L. A. N-Acetylcysteine (D- and L-Stereoisomers) Prevents Apoptotic Death of Neuronal Cells. *J. Neurosci.* **1995**, *15*, 2857–2866.
- Erickson, M. A.; Hansen, K.; Banks, W. A. Inflammation-Induced Dysfunction of the Low-Density Lipoprotein Receptor-Related Protein-1 at the Blood-Brain Barrier: Protection by the Antioxidant N-Acetylcysteine. *Brain Behav. Immun.* **2012**, *26*, 1085–1094.
- Arfsten, D. P.; Johnson, E. W.; Wilfong, E. R.; Jung, A. E.; Bobb, A. J. Distribution of Radio-Labeled N-Acetyl-L-Cysteine in Sprague-Dawley Rats and Its Effect on Glutathione Metabolism Following Single and Repeat Dosing by Oral Gavage. *Cutaneous Ocul. Toxicol.* **2007**, *26*, 113–134.
- Tortorici, M. A.; Kochanek, P. M.; Poloyac, S. M. Effects of Hypothermia on Drug Disposition, Metabolism, and Response: A Focus of Hypothermia-Mediated Alterations on the Cytochrome P450 Enzyme System. *Crit. Care Med.* **2007**, *35*, 2196–2204.
- Zhou, J.; Poloyac, S. M. The Effect of Therapeutic Hypothermia on Drug Metabolism and Response: Cellular Mechanisms to Organ Function. *Expert Opin. Drug Metab. Toxicol.* **2001**, *7*, 803–816.

21. van den Broek, M. P.; Groenendaal, F.; Egberts, A. C.; Rademaker, C. M. Effects of Hypothermia on Pharmacokinetics and Pharmacodynamics: A Systematic Review of Preclinical and Clinical Studies. *Clin. Pharmacokinet.* **2010**, *49*, 277–294.
22. Menjoge, A. R.; Kannan, R. M.; Tomalia, D. A. Dendrimer-Based Drug and Imaging Conjugates: Design Considerations for Nanomedical Applications. *Drug Discovery Today* **2010**, *15*, 171–185.
23. Kannan, S.; Dai, H.; Navath, R. S.; Balakrishnan, B.; Jyoti, A.; Janisse, J.; Romero, R.; Kannan, R. M. Dendrimer-Based Postnatal Therapy for Neuroinflammation and Cerebral Palsy in a Rabbit Model. *Sci. Transl. Med.* **2012**, *4*, 130ra46.
24. Dai, H.; Navath, R. S.; Balakrishnan, B.; Guru, B. R.; Mishra, M. K.; Romero, R.; Kannan, R. M.; Kannan, S. Intrinsic Targeting of Inflammatory Cells in the Brain by Polyamidoamine Dendrimers upon Subarachnoid Administration. *Nanomedicine* **2010**, *5*, 1317–1329.
25. Iezzi, R.; Guru, B. R.; Glybina, I. V.; Mishra, M. K.; Kennedy, A.; Kannan, R. M. Dendrimer-Based Targeted Intravitreal Therapy for Sustained Attenuation of Neuroinflammation in Retinal Degeneration. *Biomaterials* **2012**, *33*, 979–988.
26. Redmond, J. M.; Zehr, K. J.; Blue, M. E.; Lange, M. S.; Gillinov, A. M.; Troncoso, J. C.; Cameron, D. E.; Johnston, M. V.; Baumgartner, W. A. AMPA Glutamate Receptor Antagonism Reduces Neurologic Injury after Hypothermic Circulatory Arrest. *Ann. Thorac. Surg.* **1995**, *59*, 579–584.
27. Redmond, J. M.; Gillinov, A. M.; Zehr, K. J.; Blue, M. E.; Troncoso, J. C.; Reitz, B. A.; Cameron, D. E.; Johnston, M. V.; Baumgartner, W. A. Glutamate Excitotoxicity: A Mechanism of Neurologic Injury Associated with Hypothermic Circulatory Arrest. *J. Thorac. Cardiovasc. Surg.* **1994**, *107*, 776–786 discussion 786–787.
28. Rothman, S. M.; Olney, J. W. Glutamate and the Pathophysiology of Hypoxic-Ischemic Brain Damage. *Ann. Neurol.* **1986**, *19*, 105–111.
29. Tseng, E. E.; Brock, M. V.; Lange, M. S.; Blue, M. E.; Troncoso, J. C.; Kwon, C. C.; Lowenstein, C. J.; Johnston, M. V.; Baumgartner, W. A. Quantitative Analysis of Intracerebral Excitatory Amino Acids and Citrulline Following Hypothermic Circulatory Arrest. *Surg. Forum* **1997**, *48*, 297–299.
30. Teshima, Y.; Akao, M.; Li, R. A.; Chong, T. H.; Baumgartner, W. A.; Johnston, M. V.; Marbán, E. Mitochondrial ATP-Sensitive Potassium Channel Activation Protects Cerebellar Granule Neurons from Apoptosis Induced by Oxidative Stress. *Stroke* **2003**, *34*, 1796–1802.
31. Christensen, T.; Diemer, N. H. Reduction of Mitochondrial Electron Transport Complex Activity Is Restricted to the Ischemic Focus after Transient Focal Cerebral Ischemia in Rats: A Histochemical Volumetric Analysis. *Neurochem. Res.* **2003**, *28*, 1805–12.
32. Penrice, J.; Lorek, A.; Cady, E. B.; Amess, P. N.; Wylezinska, M.; Cooper, C. E.; D'Souza, P.; Brown, G. C.; Kirkbride, V.; Edwards, A. D.; et al. Proton Magnetic Resonance Spectroscopy of the Brain during Acute Hypoxia-Ischemia and Delayed Cerebral Energy Failure in the Newborn Piglet. *Pediatr. Res.* **1997**, *41*, 795–802.
33. van Harten, A. E.; Scheeren, T. W.; Absalom, A. R. A Review of Postoperative Cognitive Dysfunction and Neuroinflammation Associated with Cardiac Surgery and Anaesthesia. *Anaesthesia* **2012**, *67*, 280–293.
34. Hudetz, J. A.; Gandhi, S. D.; Iqbal, Z.; Patterson, K. M.; Pagel, P. S. Elevated Postoperative Inflammatory Biomarkers Are Associated with Short- and Medium-Term Cognitive Dysfunction after Coronary Artery Surgery. *J. Anesth.* **2011**, *25*, 1–9.
35. Parolari, A.; Camera, M.; Alamanni, F.; Naliato, M.; Polvani, G. L.; Agrifoglio, M.; Brambilla, M.; Biancardi, C.; Mussoni, L.; Biglioli, P.; et al. Systemic Inflammation after On-Pump and Off-Pump Coronary Bypass Surgery: A One-Month Follow-up. *Ann. Thorac. Surg.* **2007**, *84*, 823–828.
36. Terrando, N.; Eriksson, L. I.; Ryu, J. K.; Yang, T.; Monaco, C.; Feldmann, M.; Jonsson Fagerlund, M.; Charo, I. F.; Akassoglou, K.; Maze, M. Resolving Postoperative Neuroinflammation and Cognitive Decline. *Ann. Neurol.* **2011**, *70*, 986–995.
37. Sharief, M. K.; Thompson, E. J. In Vivo Relationship of Tumor Necrosis Factor-alpha to Blood-Brain Barrier Damage in Patients with Active Multiple Sclerosis. *J. Neuroimmunol.* **1992**, *38*, 27–33.
38. Jungwirth, B.; Eckel, B.; Blobner, M.; Kellermann, K.; Kochs, E. F.; Mackensen, G. B. The Impact of Cardiopulmonary Bypass on Systemic Interleukin-6 Release, Cerebral Nuclear Factor-kappa B Expression, and Neurocognitive Outcome in Rats. *Anesth. Analg.* **2010**, *110*, 312–320.
39. Langdon, K. D.; Granter-Button, S.; Corbett, D. Persistent Behavioral Impairments and Neuroinflammation Following Global Ischemia in the Rat. *Eur. J. Neurosci.* **2008**, *28*, 2310–2318.
40. Barron, K. D. The Microglial Cell. A Historical Review. *J. Neurol. Sci.* **1995**, *134*, 57–68.
41. Dommergues, M. A.; Plaisant, F.; Verney, C.; Gressens, P. Early Microglial Activation Following Neonatal Excitotoxic Brain Damage in Mice: A Potential Target for Neuroprotection. *Neuroscience* **2003**, *121*, 619–628.
42. McRae, A.; Gilland, E.; Bona, E.; Hagberg, H. Microglia Activation after Neonatal Hypoxic-Ischemia. *Brain Res. Dev. Brain Res.* **1995**, *84*, 245–252.
43. Gehrmann, J.; Matsumoto, Y.; Kreutzberg, G. W. Microglia: Intrinsic Immuneffectector Cell of the Brain. *Brain Res. Rev.* **1995**, *20*, 269–287.
44. Regen, T.; van Rossum, D.; Scheffel, J.; Kastriti, M. E.; Revelo, N. H.; Prinz, M.; Brück, W.; Hanisch, U. K. CD14 and TRIF Govern Distinct Responsiveness and Responses in Mouse Microglial TLR4 Challenges by Structural Variants of LPS. *Brain Behav. Immun.* **2011**, *25*, 957–970.
45. Hayder, M.; Poupop, M.; Baron, M.; Nigon, D.; Turrin, C. O.; Caminade, A. M.; Majoral, J. P.; Eisenberg, R. A.; Fournié, J. J.; Cantagrel, A.; et al. A Phosphorus-Based Dendrimer Targets Inflammation and Osteoclastogenesis in Experimental Arthritis. *Sci. Transl. Med.* **2011**, *3*, 81ra35.
46. Kobayashi, H.; Brechbiel, M. W. Nano-Sized MRI Contrast Agents with Dendrimer Cores. *Adv. Drug Delivery Rev.* **2005**, *57*, 2271–2286.
47. Malik, N.; Wiwatthanapatapee, R.; Klopsch, R.; Lorenz, K.; Frey, H.; Weener, J. W.; Meijer, E. W.; Paulus, W.; Duncan, R. Dendrimers: Relationship between Structure and Biocompatibility *in Vitro*, and Preliminary Studies on the Bio-distribution of <sup>125</sup>I-Labelled Polyamidoamine Dendrimers *in Vivo*. *J. Controlled Release* **2000**, *65*, 133–148.
48. Greish, K.; Thiagarajan, G.; Herd, H.; Price, R.; Bauer, H.; Hubbard, D.; Burckle, A.; Sadekar, S.; Yu, T.; Anwar, A.; et al. Size and Surface Charge Significantly Influence the Toxicity of Silica and Dendritic Nanoparticles. *Nanotoxicology* **2012**, *6*, 713–723.
49. Sadekar, S.; Ray, A.; Janat-Amsbury, M.; Peterson, C. M.; Ghadehari, H. Comparative Biodistribution of PAMAM Dendrimers and HPMA Copolymers in Ovarian-Tumor-Bearing Mice. *Biomacromolecules* **2011**, *12*, 88–96.
50. de Vries, H. E.; Kuiper, J.; de Boer, A. G.; Van Berk, T. J.; Breimer, D. D. The Blood-Brain Barrier in Neuroinflammatory Diseases. *Pharmacol. Rev.* **1997**, *49*, 143–155.
51. Petty, M. A.; Lo, E. H. Junctional Complexes of the Blood-Brain Barrier: Permeability Changes in Neuroinflammation. *Prog. Neurobiol.* **2002**, *68*, 311–323.
52. Mishra, M. K.; Kotta, K.; Hali, M.; Wykes, S.; Gerard, H. C.; Hudson, A. P.; Whittum-Hudson, J. A.; Kannan, R. M. PA-MAM Dendrimer-Azithromycin Conjugate Nanodevices for the Treatment of *Chlamydia trachomatis* Infections. *Nanomedicine* **2011**, *7*, 935–944.
53. Perumal, O. P.; Inapagolla, R.; Kannan, S.; Kannan, R. M. The Effect of Surface Functionality on Cellular Trafficking of Dendrimers. *Biomaterials* **2008**, *29*, 3469–3476.
54. Lesniak, W. G.; Mishra, M. K.; Jyoti, A.; Balakrishnan, B.; Zhang, F.; Nance, E.; Romero, R.; Kannan, S.; Kannan, R. M. Biodistribution of Fluorescently Labeled PAMAM Dendrimers in Neonatal Rabbits: Effect of Neuroinflammation. *Mol. Pharmacol.* **2013**, *10*, 4560–4571.
55. Navath, R. S.; Kurtoglu, Y. E.; Wang, B.; Kannan, S.; Romero, R.; Kannan, R. M. Dendrimer—Drug Conjugates for Tailored Intracellular Drug Release Based on Glutathione Levels. *Bioconjugate Chem.* **2008**, *19*, 2446–2455.

56. Kurtoglu, Y. E.; Navath, R. S.; Wang, B.; Kannan, S.; Romero, R.; Kannan, R. M. Poly(amiidoamine) Dendrimer–Drug Conjugates with Disulfide Linkages for Intracellular Drug Delivery. *Biomaterials* **2009**, *30*, 2112–2121.
57. Duncan, R.; Izzo, L. Dendrimer Biocompatibility and Toxicity. *Adv. Drug Delivery Rev.* **2005**, *57*, 2215–2237.
58. Thiagarajan, G.; Greish, K.; Ghandehari, H. Charge Affects the Oral Toxicity of Poly(amiidoamine) Dendrimers. *Eur. J. Pharm. Biopharm.* **2013**, *84*, 330–334.
59. Loscher, W.; Esenwein, H. Pharmacokinetics of Sodium Valproate in Dog and Mouse. *Arzneimittelforschung*. **1978**, *28*, 782–787.
60. Golden, P. L.; Brouwer, K. R.; Pollack, G. M. Assessment of Valproic Acid Serum-Cerebrospinal Fluid Transport by Microdialysis. *Pharm. Res.* **1993**, *10*, 1765–1771.
61. Markowitz, G. J.; Kadam, S. D.; Boothe, D. M.; Irving, N. D.; Comi, A. M. The Pharmacokinetics of Commonly Used Antiepileptic Drugs in Immature CD1 Mice. *NeuroReport* **2010**, *21*, 452–456.
62. Dixon, J. A.; Spinale, F. G. Development of Therapeutics for Heart Failure: Large Animal Models of Heart Failure—A Critical Link in the Translation of Basic Science to Clinical Practice. *Circ.: Heart Failure* **2009**, *2*, 262–271.
63. Wu, W.; Goldstein, G.; Adams, C.; Matthews, R. H.; Ercal, N. Separation and Quantification of N-Acetyl-L-cysteine and N-Acetyl-cysteine-amide by HPLC with Fluorescence Detection. *Biomed. Chromatogr.* **2006**, *20*, 415–422.
64. Gaies, M. G.; Gurney, J. G.; Yen, A. H.; Napoli, M. L.; Gajarski, R. J.; Ohye, R. G.; Charpie, J. R.; Hirsch, J. C. Vasoactive-Inotropic Score as a Predictor of Morbidity and Mortality in Infants after Cardiopulmonary Bypass. *Pediatr. Crit. Care Med.* **2010**, *11*, 234–238.
65. Wernovsky, G.; Wypij, D.; Jonas, R. A.; Mayer, J. E., Jr.; Hanley, F. L.; Hickey, P. R.; Walsh, A. Z.; Chang, A. C.; Castañeda, A. R.; Newburger, J. W.; et al. Postoperative Course and Hemodynamic Profile after the Arterial Switch Operation in Neonates and Infants. A Comparison of Low-Flow Cardiopulmonary Bypass and Circulatory Arrest. *Circulation* **1995**, *92*, 2226–2235.
66. Tisherman, S. A.; Safar, P.; Radovsky, A.; Peitzman, A.; Marrone, G.; Kuboyama, K.; Weinrauch, V. Profound Hypothermia (less than 10°C) Compared with Deep Hypothermia (15 degrees C) Improves Neurologic Outcome in Dogs After Two Hours' Circulatory Arrest Induced to Enable Resuscitative Surgery. *J. Trauma* **1991**, *31*, 1051–1061 discussion 1061–1062.